

Characterization of Manganese Oxides/Au Nanocomposite Thin Films for Supercapacitor

Jiun-Shing Liu, Yi Hu*

Department of Materials Engineering, Tatung University, Taipei, Taiwan, R.O.C.

*E-mail: huyi@ttu.edu.tw

Received: 1 February 2013 / Accepted: 24 May 2013 / Published: 1 July 2013

Nanocomposite of manganese oxides/Au thin films were electrodeposited on ITO glass substrate by the potentiostatic method in $\text{KMnO}_4/\text{AuCl}_3$ aqueous solution. The thickness of the thin films was about 50~100nm composed of manganese oxide nanoparticles. MnOOH formed as the primary phase under electrodeposition without Au addition. The films exhibit the mixture of amorphous $\text{MnO}_2 \cdot n\text{H}_2\text{O}$ and MnOOH phases under electrodeposition with Au addition. The nanocomposite thin films were characterized by scanning electron microscopy, transmission electron microscopy, X-ray photoelectron spectroscopy, cyclic voltammetry and impedance spectroscopy. The electrodes with 0.8% Au showed excellent capacitive behavior in the 0.1 M KNO_3 electrolyte, with highest specific capacitance of 1230 Fcm^{-3} at a scan rate of 20 mVs^{-1} . The nanocomposite films became looser with lots of small crevices when Au was added from the SEM surface morphology observation. This gives smaller diffusion impedance and larger capacitance through the interconnected pores for proton diffusion.

Keywords: nanocomposite, manganese oxide, gold, supercapacitor

1. INTRODUCTION

The supercapacitors or Electrochemical capacitors (ECs) in general exhibit high power density and will become more necessary for applications [1-3]. Many researches on the supercapacitors aim to increase power and energy density as well as to lower fabrication cost. Various transition-metal oxides have been identified as possible electrode materials for ECs. Among the many transition-metal oxide materials, manganese oxide is being considered as one of the promising potential electrode materials for an EC due to its low cost, environmental compatibility, and good electrochemical performances [4, 5]. Several studies have been carried out on amorphous or nanocrystallized MnO_2 compounds obtained by the sol-gel route [6,7], chemical precipitation [8,9] or electrodeposition [10,11]. Since electrochemical deposition is simple and controllable technique, many investigations have applied this

technique on the preparation of manganese dioxide films [12,13]. In this work, the manganese oxide films were electrodeposited by the potentiostatic methods from potassium permanganate solutions.

However, the reported specific capacitance values for various nanostructured manganese oxide electrodes are still far below the theoretical value [14]. This is attributed to the poor electronic conductivity of the manganese oxides. Consequently, it becomes necessary to improve the capacitive performance of manganese oxides by adding conductive additives to improve the electron transport [15-19]. Recently, carbon nanotubes (CNTs) and conducting polymers have been intensively used with MnO_2 to make nanocomposites and have reported a high specific capacitance and rate capability [20-25]. In the present study we synthesized manganese oxide thin films combined with Au nanoparticles by an electrochemical method to improve the electronic conductivity. Au particles can be inserted into manganese oxide thin films by electrochemical method. To our knowledge, the fabrication of Au into manganese oxide thin films has not been reported in literature.

2. EXPERIMENTAL

The nanocomposite thin films were obtained by electrodeposition with potentiostatic method. The solution for the electrodeposition was prepared with reagent grade potassium permanganate (KMnO_4) and gold chloride (AuCl_3) dissolved in deionized water. The concentration of potassium permanganate was kept as 0.01M and the molar ratio of the Au/Mn in the solution varied from 0 to 1.6%. The thin films were cathodically electrodeposited on the ITO glass substrate with -0.7V v.s. open circuit for 200s at room temperature. The morphology of the thin films were studied using a field emission scanning electronic microscope (FESEM, Hitachi S-4700). Transmission Electron Microscopy (TEM) analyses were performed using a JEOL JEM-1200EX electron microscope operated at 200 kV. The states of the ions were investigated by X-ray photoelectron spectroscopy (XPS, VG ESCA Scientific Theta Probe) with Al $K\alpha$ (1486.6eV) and the X-ray spot size is 15 μm .

The electrochemistry behavior of the cell was examined by the cyclic voltammetry with conventional three-electrode system using the electrochemical tested system (Electrochemical station 5000 Jiehan). The counter electrode was platinum gauze and the reference electrode was a standard calomel reference electrode (SCE). The measurement of cyclic voltammetry (CV) was conducted from 0 to 1.0 V with scan rates of 20 mVs^{-1} and the electrolyte was 0.1M KNO_3 . The cell for impedance measurement is made with a sandwich structure, the outset is the glass, the second layer is the gold/manganese oxides thin film electrode, the mesosphere is a polymer electrolyte membrane used as separator. KNO_3 (0.1 M) in distilled water was used as the electrolyte. This experiment was conducted with an impedance spectroscopy (Hioki 3522-50 LCR hitester). It was polarized with 0.5 constant voltage. The ripple frequency was swept between 1Hz and 0.1M Hz.

3. RESULTS AND DISCUSSION

Figure 1 shows the typical SEM images of the samples. The thickness of the thin films are in the range of 50~100nm observed from the cross-sectional SEM images as in Fig, 1(a). It was found

that the thickness of the films decreased as the Au content increased. These films were composed of nanoparticles in the range of 10~30nm as seen in Fig. 1(b) ~ (d). The size of the nanoparticles seems to increase with the increase of Au content. In addition, the surface morphology of the thin film became looser with lots of small crevices when Au was added.

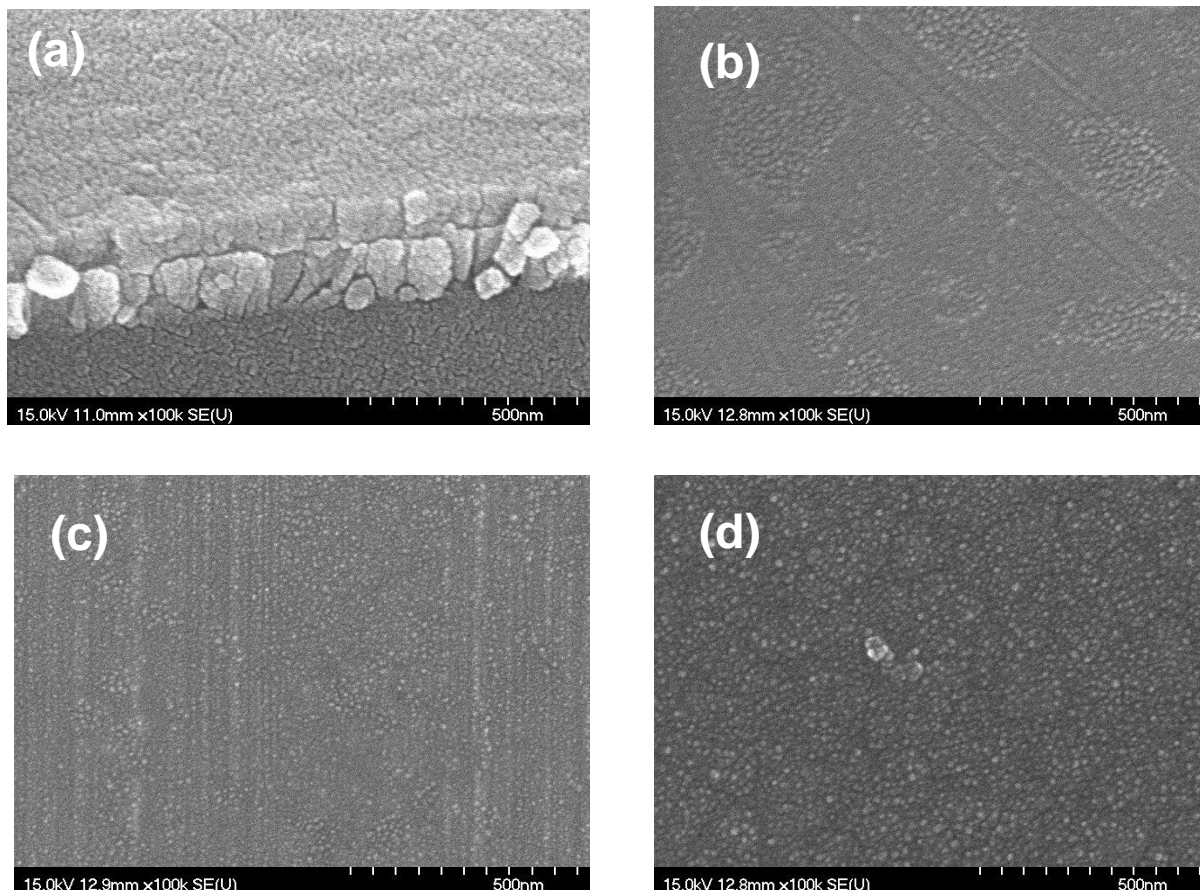


Figure 1. (a) Typical cross-sectional SEM image of the nanocomposite thin film, and surface SEM images of the thin films with the Au/ Mn ratio of (b) 0%, (c)0.4%, (d)18%.

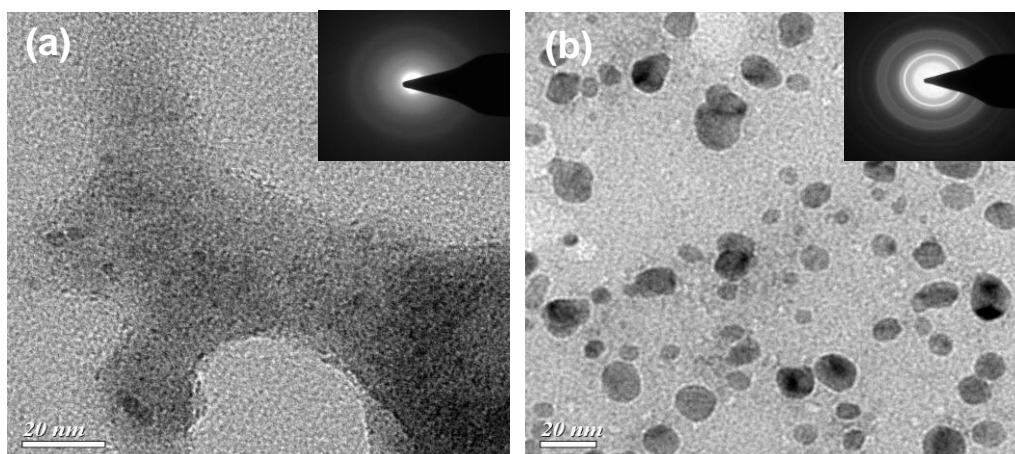


Figure 2. Typical TEM images with inserted diffraction patterns of the thin films. (a) without Au and (b) with Au/Mn ratio of 1.6% (b).

Figure 2 shows the typical TEM images of the thin films with and without Au addition. The thin film without Au addition is shown to be amorphous evidenced from the diffuse features in the diffraction pattern as in Fig. 2(a). On the other hand, distinctive images of gold particles appeared as small dark spherical shapes or dots in the thin film as in Fig. 2(b). The average size of the Au particles was close to 15 nm based on the TEM image. The gold nanoparticles are crystalline and metallic with face centered cubic structure determined from the diffraction pattern as in Fig. 2(b).

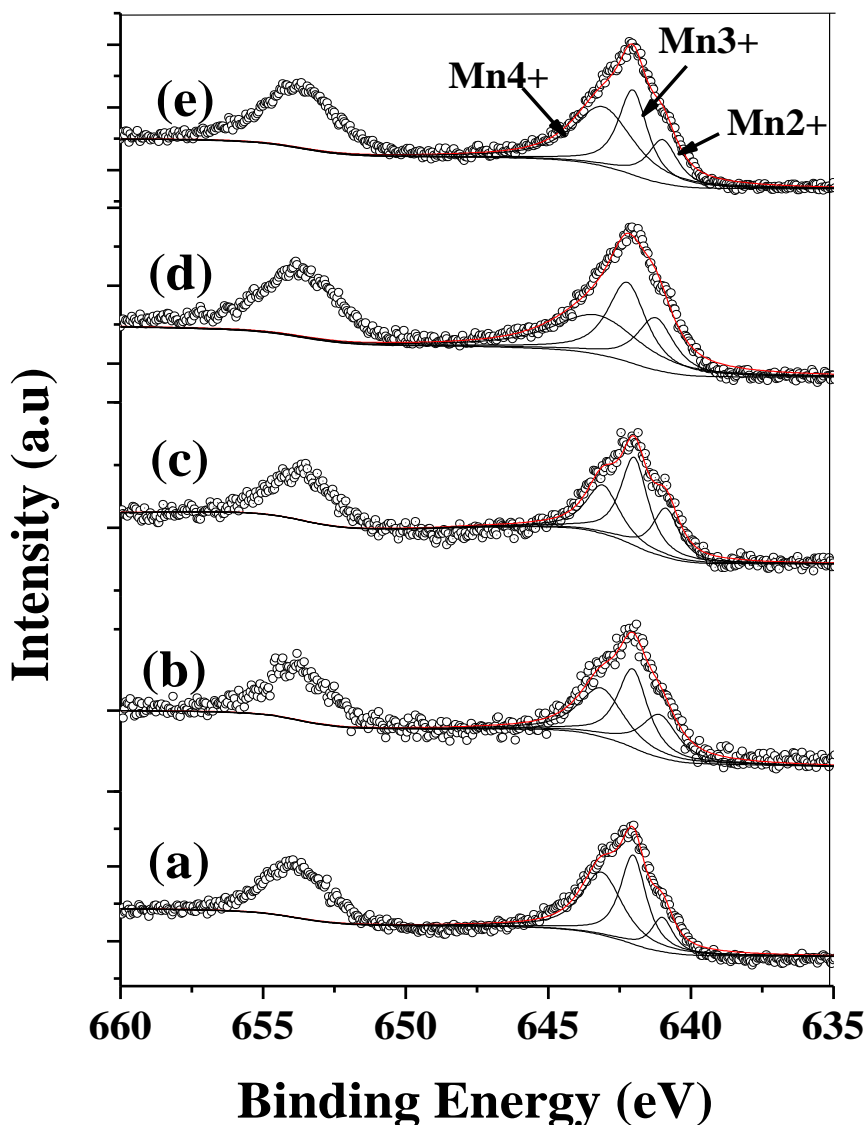


Figure 3. Mn $2p_{3/2}$ and Mn $2p_{1/2}$ XPS spectra for the nanocomposite thin films versus Au/Mn ratio of (a) 0% (b) 0.2% (c) 0.4% (d) 0.8% (e) 1.6%

The nanocomposite samples were characterized further using XPS analysis. Figure 3 shows the XPS spectra with peak-fit processing for Mn $2p_{3/2}$ and Mn $2p_{1/2}$ of the samples with different Au content. It is found that the main binding energy of Mn $2p_{3/2}$ peak is at about 642.0 eV. However,

three peaks were found from differentiation of the original peak with binding energy at 640.95, 641.99, and 643.05 eV. This is consistent to the binding energy of the Mn 2p_{3/2} for the pure manganese oxides, such as 640.9eV for the MnO, 641.9 eV for the α -Mn₂O₃, 642.5 eV for the β -MnO₂ and 643~643.6 eV for the Mn⁵⁺ [26, 27]. Therefore, it can be inferred that there are about three kinds of ion state as Mn²⁺, Mn³⁺, and Mn⁴⁺ in the thin films. Higher oxidation state of manganese would have higher binding energy. No shift of the Mn2p peaks was observed from the XPS patterns. This indicates that the fraction of each manganese ion state does not change noticeably with Au addition.

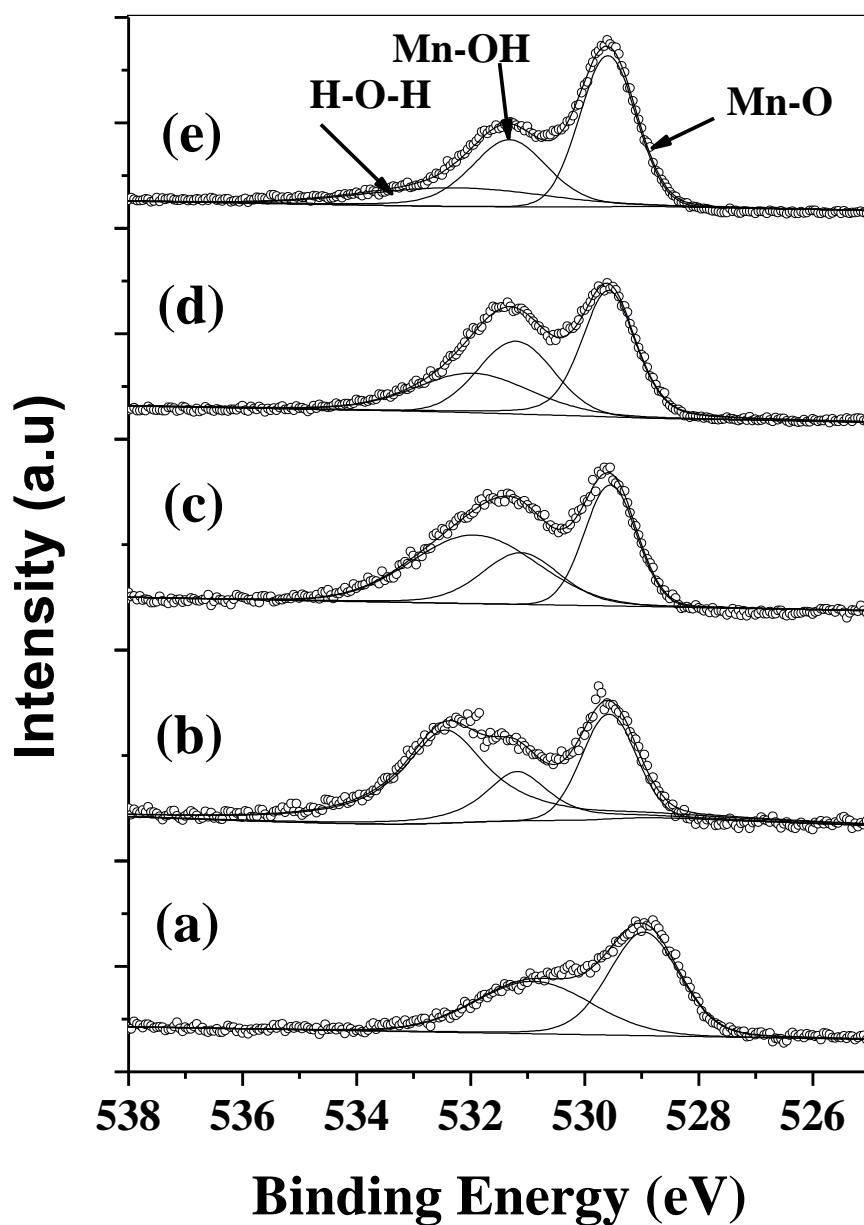


Figure 4. O1s XPS spectra for the nanocomposite thin films versus Au/Mn ratio of (a) 0% (b) 0.2% (c) 0.4% (d) 0.8% (e) 1.6%

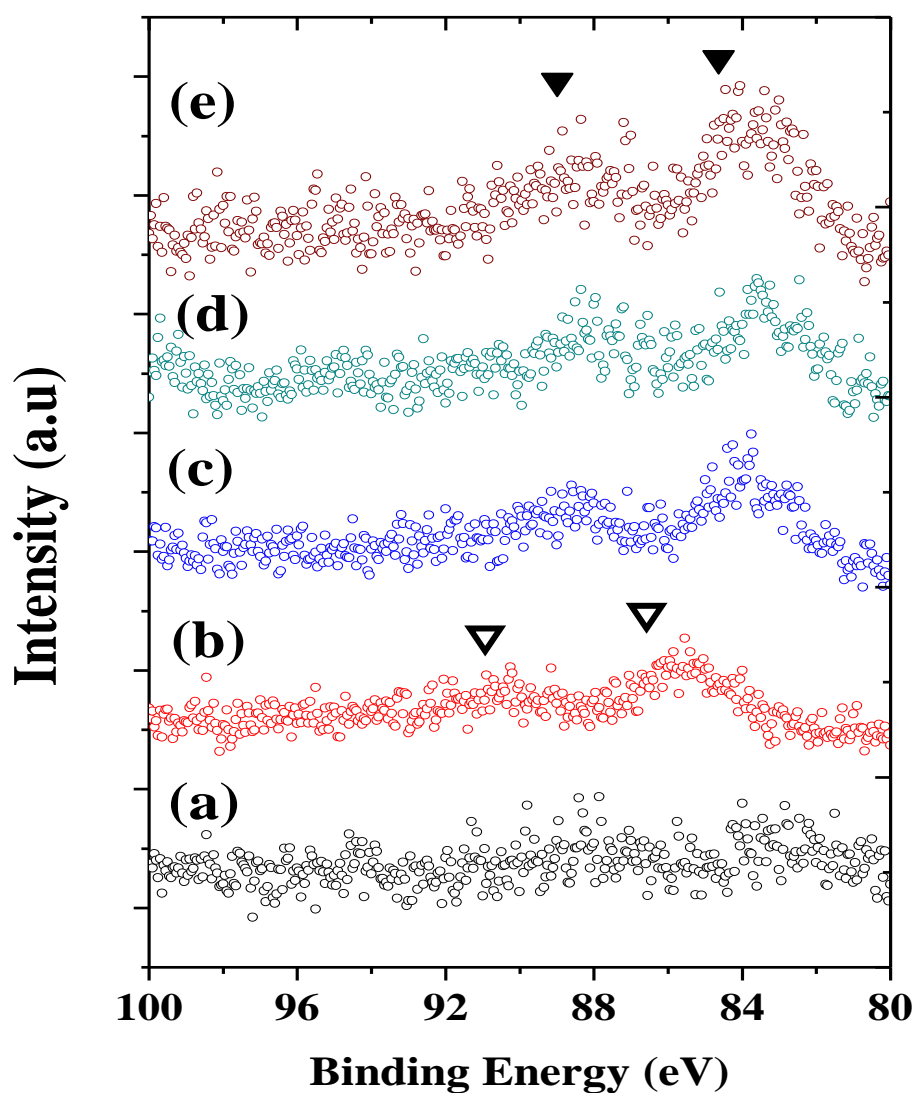


Figure 5. Au $4f_{7/2}$ and Au $4f_{5/2}$ XPS spectra for the nanocomposite thin films versus Au/Mn ratio of (a) 0% (b) 0.2% (c) 0.4% (d) 0.8% (e) 1.6%

The O1s XPS spectra with peak-fit processing of the samples are shown in Fig. 4. There are three oxygen-containing binding energy of the O $1s_{1/2}$ for the samples as Mn oxide (Mn-O-Mn) at 529.3-530.3 eV, the hydroxyl (Mn-OH) at 530.5-531.5 eV, and residual structure water (H-O-H) at 531.8-532.8 eV [28-31]. It can be inferred that MnOOH formed as the primary phase under electrodeposition without Au addition. As the gold was added, the H-O-H bond was apparently perceived. Nevertheless, the intensity of Mn-O-H bond increased, whereas the intensity of the H-O-H bond decreased as the Au content increased. This indicates that amorphous $MnO_2 \cdot nH_2O$ became the predominant phase under electrodeposition with Au addition. The films exhibit the mixture of

amorphous $\text{MnO}_2 \cdot n\text{H}_2\text{O}$ and MnOOH phases with Au addition. However, the volume fraction of amorphous MnOOH increased under electrodeposition with further addition of Au.

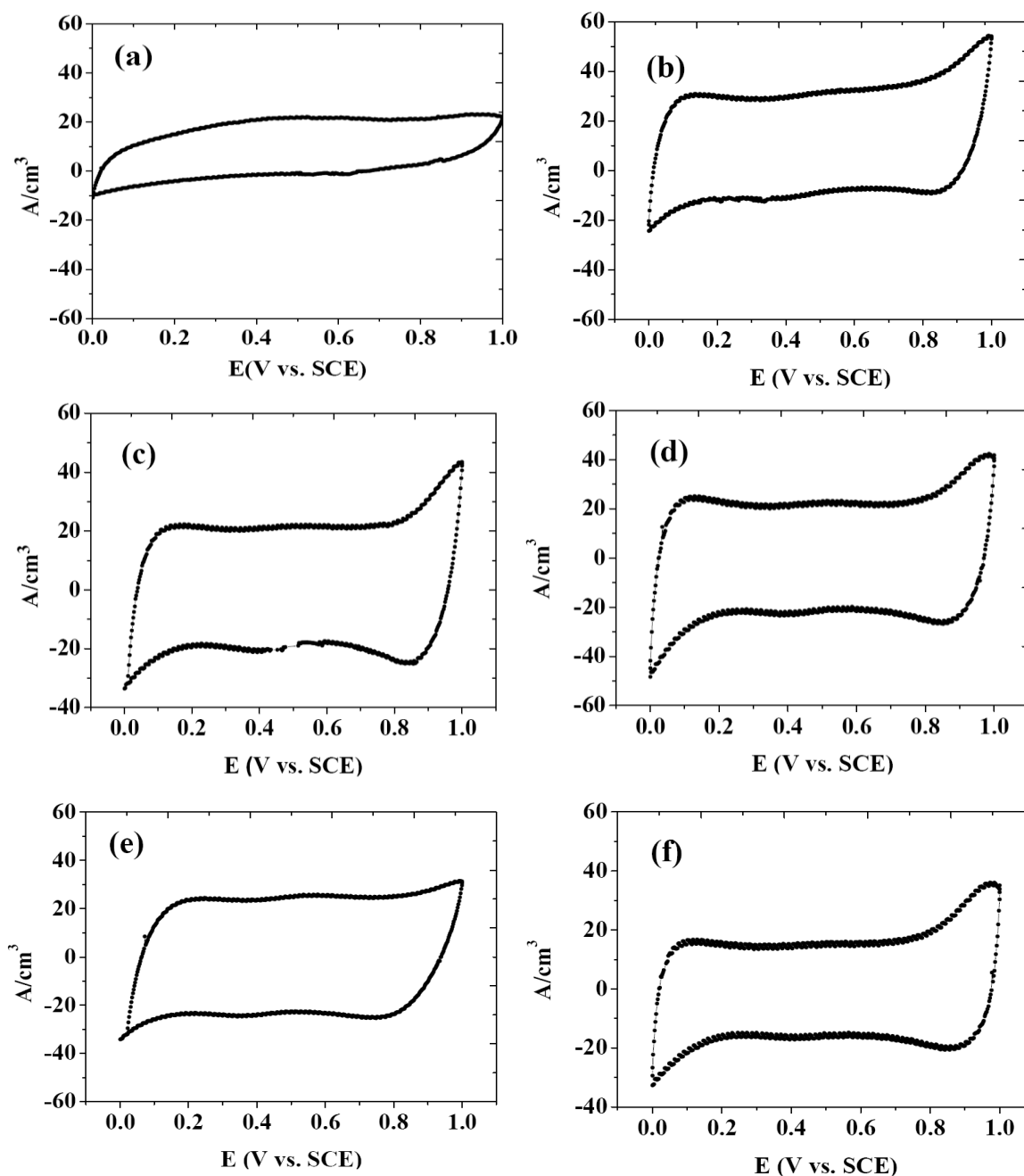
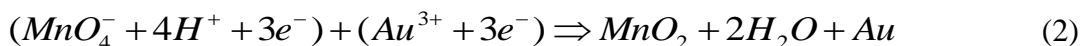


Figure 6. The cyclic voltammetry of the samples with Au/ Mn ratio of (a) 0%, (b) 0.2%, (c) 0.4%, (d) 0.8%, (e) 1.6% at a scan rate of 20 mV s^{-1} .

Figure 5 shows Au 4f XPS spectra of the samples. Two peaks at energies of 85.5 and 89.4 eV for the sample with 2% Au were found in Fig. 5(b). This is from that the Au is bonded to O in an Au_2O_3 structure as reported in the literature [32-34]. On the other hand, the Au $4f_{7/2}$ and Au $4f_{5/2}$ levels give rise to peaks positioned at 83.7 eV and 87.4 eV respectively as pure gold [35,36] for the

sample with higher Au content as in Fig. 5(c)~(e). The state of Au nanoparticles in the thin films appears as atomic state and is consistent with the value of pure Au.

Manganese oxide films were cathodically deposited by reduction of KMnO_4 . It is suggested that the following reactions deduced from the results can give rise to the reduction of MnO_4^- :



Amorphous MnOOH is the primary phase formed by the reaction with proton under electrodeposition as shown in eq. (1). This suggests that the electrodeposition process involves a two-electron transfer mechanism as written. However, addition of Au would cause the formation of MnO_2 as in eq.(2) under further reduction process with a three-electron transfer mechanism. In addition, water molecules may incorporate into the oxide film during electrodeposition as observed from the XPS patterns.

Figure 6 shows the CV curves of nanocomposite samples in a 0.1M KNO_3 solution at room temperature at the scanning rate from 20 mV s^{-1} . The CV curve for the sample without Au addition shows non-rectangle-shaped smooth circle as in Fig. 6(a). In Fig.6 (b) ~ (e), the CV curve shows the rectangle-like shape, indicating the good electrochemical characteristics of the sample with Au addition. In addition, the CV curves present a small redox peaks nearly at 0.50 V (vs. SCE), which can be assigned to the proton or alkali ions deintercalation upon oxidation and intercalation upon reduction [37]. The overall reaction has been proposed and generally can be expressed as follow [1]:



The relatively high charge-storage capacity of manganese dioxide is presumably due to proton diffusion into hydrous manganese dioxide films.

The specific capacitance (SC) of the sample is determined from the CV data. The plots of SC are shown in Fig.7 as a function of Au content. The SC value of the sample as found increased as the ratio of the Au/Mn increased up to 0.8 and then the SC decreased as further increased Au content. The SC of the sample without Au addition is about 623 F/cm^3 . The highest capacitance was about 1230 F/cm^3 for the sample with Au/Mn=0.8wt%. It was found that the SC seemed to be as a function of the amount of water incorporated into the oxide films. This may be ascribed to the higher surface area of the porous thin film to incorporate water. In addition, the incorporated water would also give a route for proton diffusing into the manganese dioxide films. The results confirm that thin film became looser with lots of small crevices when Au was added from the SEM surface morphology observation. These cervices of the films would provide more surface area to incorporate water.

The electrochemical impedances plot of the nanocomposite electrodes are shown in Fig. 8. The internal resistance of the nanocomposite electrodes was estimated to range from 0.25 to 0.76 $\Omega\text{-cm}$ from the point intersecting with the real axis in the range of high frequency. The sample with Au

addition shows lower internal resistance than that of the sample without of Au addition. The variation of the internal resistance of the sample was attributed to the intrinsic resistance of the active material and the contact resistance at the active material/current collector interface.

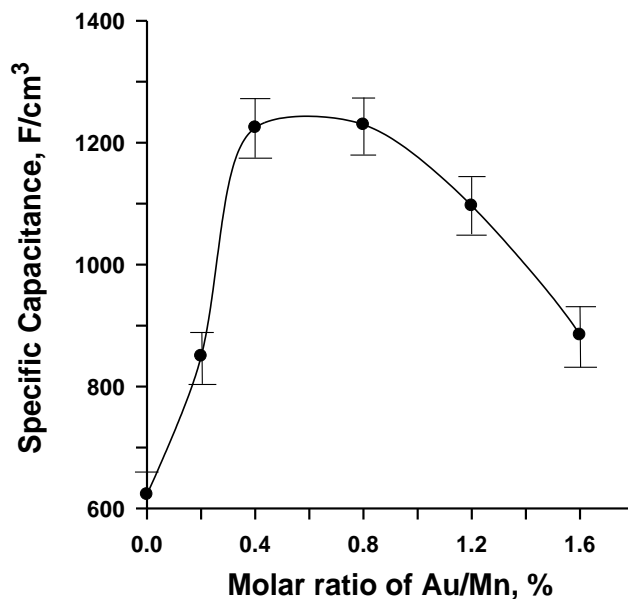


Figure 7. Specific capacitance of the sample as a function of the Au content.

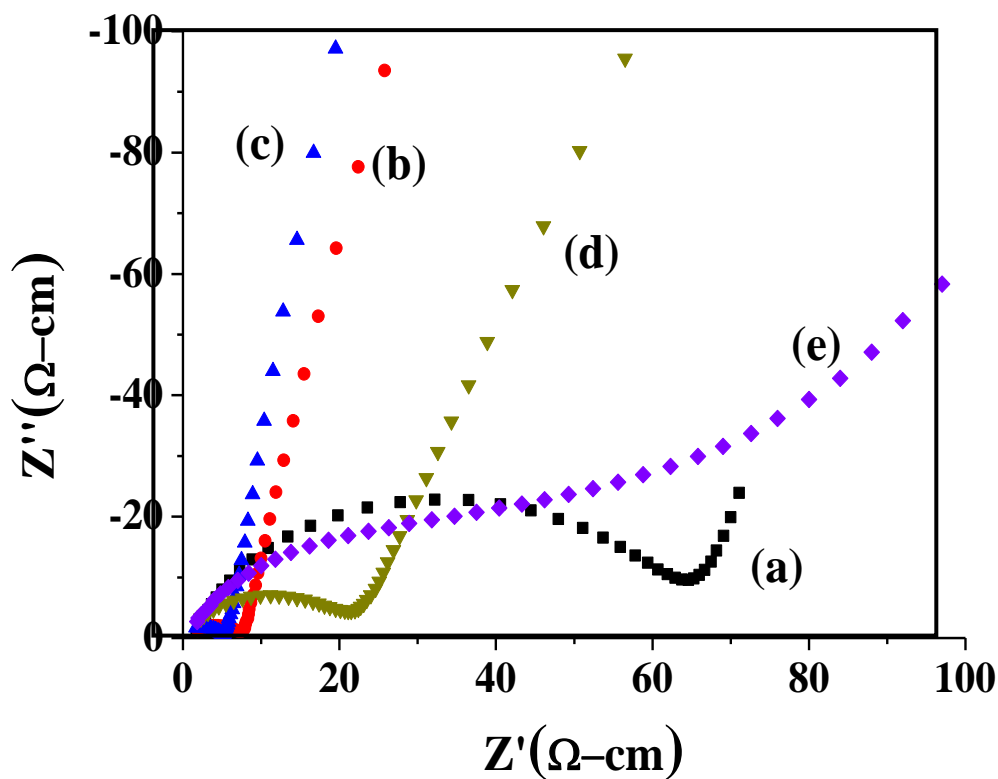


Figure 8. The Nyquist plots of the complex impedance spectra for the nanocomposite electrodes with Au/Mn ratio of (a) 0%, (b) 0.2%, (c) 0.4%, (d) 0.8%, (e) 1.6%.

On the other hand, it can be seen from Fig. 8 that all the plots are composed of a semicircle and a straight line. It has been suggested that the semicircle at higher frequency region is attributed to the charge transfer process at electrode/electrolyte interface, and the straight line at lower frequency region is due to the diffusion process in solid [1]. Apparently, the semicircle of the nanocomposite electrode became smaller with Au addition as in Fig. 8. This indicates that the electrochemical reaction resistance of nanocomposite electrode decreased with Au addition. On the other hand, the impedance plots of sample are steeper in the low frequency region with Au addition of 0.2 and 0.4%. This suggests that the cell is more capacitive by adding small amount of Au. Generally, electrode has a smaller diffusion impedance and a larger capacitance, probably due to the morphology, composed of interconnected pores. Thin film with lots of small crevices when Au was added would thus give the interconnected pores for proton diffusion. The nanostructure of the electrode has important effect on its supercapacitance. The main difference in these materials with/without Au addition is not only the amount of surface area, but how easily accessible these pores are for proton diffusion.

4. CONCLUSIONS

The pseudocapacitive charge storage reactions of the MnOOH/MnO₂·nH₂O/Au nanocomposite electrode have been investigated mainly by SEM, TEM, XPS, cyclic voltammetry and impedance spectroscopy. Amorphous MnO₂·nH₂O formed under electrodeposition with Au addition. The relatively high charge-storage capacity of manganese dioxide is presumably due to proton diffusion into hydrous manganese dioxide films. The SC of the sample without Au addition is about 623 F/cm³. The highest capacitance was about 1230 F/cm³ for the sample with Au/Mn=0.8wt%. It had been proved by the modeling results of impedance data, which showed the less charge-transfer resistance and low frequency impedance for the sample with Au addition. The better capability of the sample with Au addition may be attributed to its high surface area of porous structure, leading to the easier diffusion of proton and the more accessible active sites.

References

1. B.E. Conway, *Electrochemical Supercapacitors: Scientific Fundamentals and Technological Applications*, Kluwer Academic/Plenum Publisher, New York (1999).
2. T. Morimoto, K. Hiratsuka, Y. Sanada, K. Kurihara, *J. Power Sources*, 60 (1996) 239
3. J. Gamby, P.L. Taberna, P. Simon, J.F. Fauvarque, M. Chesneau, *J. Power Sources*, 101 (2001) 109
4. S.-C. Pang, M. A. Anderson, and T. W. Chapman, *J. Electrochem. Soc.*, 147 (2000) 444
5. M. Toupin, T. Brousse, D. Bélanger, *Chem. Mater.*, 14 (2002) 3946
6. S.C. Pang, M.A. Anderson, T.W. Chapman, *J. Electrochem. Soc.*, 147 (2000) 444
7. R.N. Reddy, R.G. Reddy, *J. Power Sources*, 124 (2003) 330
8. M. Toupin, T. Brousse, D. B'elanger, *Chem. Mater.*, 16 (2004) 3184
9. M. Toupin, T. Brousse, D. Bélanger, *Chem. Mater.*, 14 (2002) 3946
10. J. Jiang, A. Kucernak, *Electrochim. Acta*, 47 (2002) 2381
11. C.C. Hu, T.W. Tsou, *Electrochim. Acta*, 47 (2002) 3523
12. N. Nagarajan, H. Humadi, I. Zhitomirsky, *Electrochim. Acta*, 51 (2006) 3039.

13. B. Babakhani, D.G. Ivey, *J. Power Sources*, 195 (2010) 2110.
14. M. Toupin, T. Brousse, D. Bélanger, *Chem. Mater.*, 16 (2004) 3184
15. A. E. Fischer, K. A. Pettigrew, D. R. Rolison, R. M. Stroud, J. W. Long, *Nano. Lett.*, 7 (2007) 281.
16. F.-J. Liu, *Journal of Power Sources*, 182 (2008) 383
17. J. Zhou, J. Cheifetz, R. Li, F. Wang, X. Zhou, T.-K. Sham, X. Sun, Z. Ding, *Carbon* 47 (2009) 829
18. V. Subramanian, H. Zhu, B. Wei, *Electrochem. Comm.*, 8 (2006) 827
19. S.I.A. Razak, A.L. Ahmad, S.H.S. Zein, A.R. Boccaccini, *Scripta Materialia* 61 (2009) 592
20. K. H. An, K. K. Jeon, J. K. Heo, S. C. Lim, D. J. Bae, and Y. H. Lee, *J. Electrochem. Soc.*, 149 (2002) A1058
21. H. Xie, Y. Wang, J. Linand, L. Lu, *Nano. Res. Lett.*, 7 (2012) 33
22. G.-X. Wang, B.-L. Zhang, Z.-L. Yu, M.-Z. Qu, *Solid State Ionics* 176 (2005) 1169
23. Y. Wang, H. Liu, X. Sun and I. Zhitomirsk, *Scripta Materialia* 61 (2009) 1079
24. S. I. A. Razak, A. L. Ahmad and S. H. S. Zein, *J. of Phys. Sci.*, 20 (2009) 27
25. X. Zhang, L. Ji, S. Zhang, W. Yang, *J. Power Sources*, 173 (2007) 1017
26. J.S Foord, R.B. Jackman, G. C. Allen, *Philos. Mag.*, A49(1984) 657
27. W. P. Kilroy, S. Dallek, J. Zaykoski, *J. Power Sources*, 105 (2002) 75
28. J. F. Moulder, W. F. stickle, K.D. Bompén, Handbook of photoelectron spectroscopy, Perkin Elmer, Eden Praire, 1991
29. X. Han, L. Zhou, H. Liu, Y. Hu, *Polymer Degradation and Stability* 92 (2007) 75
30. M. Chigane, M. Ishikawa, *J. Electrochem. Soc.*, 147 (2000) 2246
31. D. Banerjee, H.W. Nesbitt, *Geochim. Cosmochim. Acta*, 63 (1999) 3025
32. A. Krozer, M. Rodahi, *J. Vac. Sci. Technol.*, A 15 (1997)1704
33. D. E. King, *J. Vac. Sci. Technol. A*, 13 (1995) 1247
34. B. Koslowski, H.-G. Boyen, C. Wilderrotter, G. Kastle, P. Ziemann, R. Wahrenberg, P. Oelhafen, *Surf. Sci.*, 475 (2001) 1
35. S. Dieluweit, D. Pum, U.B. Sleytr, W. Kautek, *Mater. Sci. Eng.*, 25 (2005) 727
36. G. Doderò, L.D. Michieli, O. Cavalleri, R. Rolandi, L. Oliveri, A. Dacca, R. Parodi, *Colloids Surf. A: Physicochem. Eng. Asp.*, 175 (2000) 121
37. T. Brousse, M. Toupin, R. Dugas, L. Athouel, O. Crosnier, D. Bélanger, *J. Electrochem. Soc.*, 153 (2006) A2171